Theses and Dissertations

Summer 2012

Determining the effect of congenital bicuspid aortic valves on aortic dissection using computational fluid dynamics

Jennifer Ann Burken

University of Iowa

Recommended Citation

Burken, Jennifer Ann. "Determining the effect of congenital bicuspid aortic valves on aortic dissection using computational fluid dynamics." MS (Master of Science) thesis, University of Iowa, 2012.
http://ir.uiowa.edu/etd/3270.

DETERMINING THE EFFECT OF CONGENITAL BICUSPID AORTIC VALVES ON
AORTIC DISSECTION USING COMPUTATIONAL FLUID DYNAMICS

by

Jennifer Ann Burken

A thesis submitted in partial fulfillment
of the requirements for the Master of
Science degree in Biomedical Engineering
in the Graduate College of
The University of Iowa

July 2012

Thesis Supervisors: Assistant Professor Sarah C. Vigmostad
                     Professor Krishnan B. Chandran

Graduate College
The University of Iowa
Iowa City, Iowa

CERTIFICATE OF APPROVAL

_____

MASTER'S THESIS

_____

This is to certify that the Master's thesis of

Jennifer Ann Burken

has been approved by the Examining Committee
for the thesis requirement for the Master of Science
degree in Biomedical Engineering at the July 2012 graduation.

Thesis Committee: _____
                   Sarah C. Vigmostad, Thesis Supervisor

                   _____
                   Krishnan B. Chandran, Thesis Supervisor

                   _____
                   Madhavan L. Raghavan

                   _____
                   H.S. Udaykumar

ACKNOWLEDGMENTS

I would like to express my deepest gratitude to my thesis advisors Dr. Vigmostad and Dr. Chandran for all of their support and guidance in completing this thesis. I would like to thank Dr. Udaykumar and Dr. Raghavan for agreeing to be on my committee and providing me with their expertise. Thanks also goes out to Paul and Vijay who helped create and problem solve the geometries. I would like to express my thanks to the BME secretaries April and Angie for their help with the paperwork. I am grateful or my sister Kim for her proof-reading skills. I am forever indebted to my parents, Deb and Pat, who have always encouraged me to strive, and given me their unwavering support in whatever I attempt. I would also like to thank my grandparents and the rest of family for their support. Finally I would like to thank Ben who helped proof-read, and who put up with me when I was stressed out.

ABSTRACT

A normal aortic valve has three leaflets; however, 1- 2% of children are born with an aortic valve with two leaflets, referred to as congenital bicuspid aortic valves (BAV). Recent in vivo studies have shown that flow development past the bicuspid valves into the ascending aorta is markedly different from that past the normal tri-leaflet aortic valve. This difference may lead to the bicuspid valve having a higher rate of ascending aortic root dissection, a pathology that can potentially result in fatality. Using computational fluid dynamics we aim to evaluate the alterations in flow development in the ascending aorta with BAV compared to healthy tri-leaflet valves (TAV) and relate the alterations in flow-induced stresses with higher incidences of aortic dissection in patients with BAV. Simplified models based on the geometry and dimensions from published literature were developed. The preliminary results show that there is a difference in flow development between the BAV and the tri-leaflet valve. This is visible by the differences in wall shear stress and dynamic pressure distribution in the ascending aorta. The conclusion drawn from this is that there are marked differences in the ascending aortic flow development with BAV compared to that with TAV which may lead to dissection of the aortic arch.

TABLE OF CONTENTS

'

v

LIST OF TABLES

LIST OF FIGURES

CHAPTER ONE: INTRODUCTION

1.1 Physiology

The Aorta is the major blood vessel in the body. It is connected to the heart by

the aortic valve, which is normally a Tri-leaflet valve (TAV). There are multiple sections

of the aorta. These sections are the ascending thoracic, descending thoracic, and

abdominal aorta. The aortic arch, as seen in Figure 1, consists of the ascending and

descending sections and has an intricate three dimensional curve which allows the aorta

to weave around the pulmonary vessels, esophagus, trachea, and left atria [1].
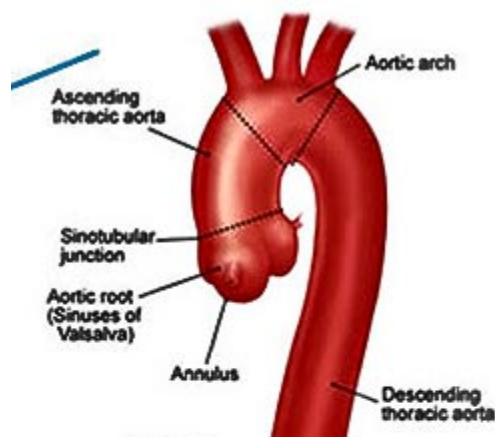
Figure 1. Sketch of the Human Aorta including the ascending and descending sections,
the Sinotubular junction and the Sinuses of Valsalva [2]

There are three bulges at the beginning of the aorta distal to the aortic valve called

the Sinuses of Valsalva. Two of the sinuses have openings that allow for blood to flow

from the aorta to the coronary arteries which supply the heart muscles with blood.

Therefore the sinuses are named for their corresponding coronary arteries. The left sinus

is called the Left Coronary sinus, the right sinus is called the Right Coronary sinus and

the final sinus is referred to as the Non-Coronary sinus because it does not have a coronary artery extending from it [3].

There is a pressure difference between the left ventricle and the aorta, which allows the aortic valve to open. During systole the fully open aortic valve allows for one directional flow from the left ventricle to the ascending aorta. Once open the blood enters the aorta in a relatively flat velocity profile [1]. During diastole when the left ventricle relaxes, the valve closes to stop the flow of blood from reversing to the left ventricle. This creates a pulsatile flow in the aorta.

The normal TAV is attached to the aortic annulus at the ascending aortic root [4]. TAV leaflets are fairly symmetrical and all three leaflets are of semicircular shape and roughly equal in size. These leaflets have an extra length of tissue as the length of the cusp between the attachment points is greater than the straight line distance between the same two points. This extra length allows the leaflets to move almost independently of each other [5].

Although a normal aortic valve has three leaflets, 1- 2% of children are born with an aortic valve with only two leaflets [6]. This is referred to as congenital bicuspid aortic valves (BAV). BAV is hypothesized to result from abnormal formation of the aortic valve during valvulogenesis in the fetus [7]. Males are at a higher risk of being born with a BAV. Although the reason for this higher risk is uncertain it is thought to be genetic [6].

There are three different types of BAV geometries that can form as seen in Figure 2. For this simulation the types of BAV leaflets were from a previous finite element (FE) study by Jermihov et al [8].
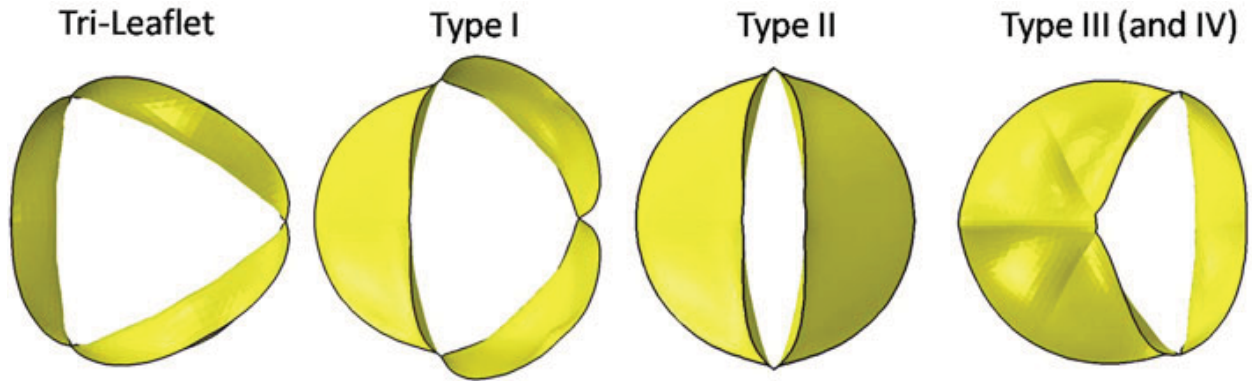
Figure 2. Types of BAV geometries that can form [8]

According to Yener et al. the most common type of BAV is Type III. This is where the left and right coronary leaflets fuse together and the non-coronary leaflet is separate [6]. The non-coronary leaflet in this type is about the same size as the normal non-coronary leaflet in the Tri-leaflet geometry [6]. Type I BAV has an oversized non-coronary leaflet and smaller left and right leaflets with a fusion of the left and right leaflets [8]. BAV Type II is referred to as a "purely bicuspid" BAV [9]. The non-coronary leaflet is oversized similar to the Type I leaflet The second leaflet has the same oversized shape and is reflected over the centerline giving two roughly equal size and shape leaflets.

The BAV geometries are not formed with the excess tissue length that the TAV has; instead the BAV leaflet length between the attachment points is the same as the straight line distance between the same two points. This limits the amount the BAV can open. Therefore the BAV is never "fully" open which reduces the effective orifice area [5]. This difference in excess tissue may result in differences in the opening and closing of the valve. Differences in opening have also been observed by Robicsek et al. who noted that the BAV folds differently than the TAV during the opening of the valve [10].

This difference of excess tissue and differences in folding in the leaflets between the normal TAV case and the BAV cases may lead to differences in flow.

<div align="center">1.2 BAV Pathology</div>

The BAV is the most common congenital heart condition [7]. It was first described in 1844 by Paget as a pathological anomaly [6]. This deformation is a cause for concern as approximately 33% of BAV patients develop serious complications [7]. Intervention, including surgery, is required by a majority of BAV patients to correct these complications during their teenage years and beyond [7].

Complications associated with BAV include: valve calcification, coarctation, dissection, and dilatation of the ascending aortic arch [6]. A study on dissecting aneurisms found that 9% of these patients had a BAV [11]. Another study with BAV male patients, who had normally functioning valves, showed that a majority had significantly larger aortic root dimensions than normal TAV patients [12].

One major complication associated with BAV is aortic dissection. It has been found that aortic dissection develops from a tear in the intimal layer of the aortic arch [13]. Nathan et al. showed that dissection is more likely to occur at points of inflection such as at the Sinotubular junction (STJ) on the inner wall of the aortic arch [14]. Aortic dissection can be caused by dilatation of the aortic root as well [7]. A study by Cecceoni et al. showed that the aortic dilatation occurred only in the ascending aorta and not in the descending aorta in BAV patients [15]. In certain cases an aortic dissection can result in fatality. In patients with TAV the chance of death from aortic dissection is between 19 and 23 %. In contrast the risk of death from aortic dissection increases to 50 % when the

patient has a BAV. Aortic dissection is shown to occur at an earlier age in patients with a

BAV than in patients with a TAV [16].

Another complication of BAV is coarctation, which is the narrowing of the aorta.

According to Edwards, eighty-five percent of patients with coarctation of the aorta have a

BAV [5]. These complications have been found to happen before the valve experiences

any other complications such as calcification. Della Corte et al. found, in a patient

population, early signs of aortic dysfunction before the valve was deformed by

complications [17].

<u>1.3 Computational Fluid Dynamics</u>

With advances in computational techniques more researchers are utilizing

computational fluid dynamics (CFD) to speed up study time and reduce animal

experimentation [18]. The method is less invasive and presents less risk to the patient

than *in-vivo* studies. CFD is usually more cost effective and simpler to use because

changes can be made faster and easier than in *in-vivo* studies. CFD also allows for more

detailed flow analysis than other experimental methods.

<u>1.4 Aim of the Present Study</u>

Using CFD this study aimed to evaluate the alterations in flow development in the

ascending aorta with the three simulated types of BAV compared to a simulated healthy

TAV and to relate the alterations in flow-induced stresses with higher incidences of aortic

dissection and disease in patients with BAV.

CHAPTER TWO: PREVIOUS STUDIES

2.1 Experimental Studies

Many studies have been completed to look at flow dynamics in a curved tube. These studies are valuable because an idealized aortic arch can be seen as a curved tube and therefore has similar properties. One study by Chandran shows the aortic arch as a curved tube with the velocity skewed toward the inner wall near the entrance to the curved tube (correlating with the ascending aorta in the aortic arch) during peak systole [1].

Multiple studies, including one by Harloff et al, have also demonstrated high wall shear stress (WSS) along the inner wall of the arch during systole [19]. In the *in-vivo* study completed by Barker et al. results showed that WSS differed significantly between BAV and control patients with TAV [20]. In a second study, completed by Della Corte et al., results showed that WSS varied along the circumference of the BAV aorta [17].

Several experimental studies have been conducted to study BAV and the diseases that are associated with it. Sievers et al. conducted a study on 304 patients who were having surgery for comorbidities that can be associated with BAV [9]. They studied the commissure, space between the leaflets, in the BAV patients. The study found that the fusion of the leaflets, the process that creates a BAV instead of a TAV, happens between two leaflets at the commissure and may result in a partial or full fusion between the leaflets. They also studied the aortic root after the BAV and found that patients with BAV still have three Sinuses of Valsalva [9].

Chandran observed that the geometry and orientation of the valves seem to affect the flow at the aortic root [1]. Schafer et al. found related results stating that there is a

possibility that the orientation of a BAV could result in different jet shapes between the BAV types [21]. Weinberg et al. also saw a difference in jets between the TAV and BAV Type II case. This jet was hypothesized to occur because the BAV leaflet formed kinks when fully open [22]. Della Corte et al. found that a difference in jet shapes was evident in BAV cases. This jet was skewed downstream of the non-coronary sinus and impacted at the outer wall of the aortic arch. The study also hypothesizes that the jet could cause remodeling of the wall at the impact site as it has been happening since birth [17]. Therefore different jet shapes could lead to the higher risk of patients with BAV having complications.

<u>2.2 Flow Dynamics Relating to Complications</u>

BAV has been seen to alter hemodynamics in the ascending aorta which could lead to coarctation [23]. Hope et al. performed a study that showed the BAV altered hemodynamics as well. The study showed an abnormal helical aortic flow in 75% of subjects with BAV regardless of comorbidities but none in TAV. Hope et al. hypothesized that this helical flow may lead to aneurysm formation in the aorta [24]. As mentioned before a common place of inflection for this dissection is just above the STJ where there has been shown to be an increase in wall shear stress [14]. Dilatation of the aorta in a BAV population has also shown to have a correlation between WSS and ascending aorta size [20]. Another study by Martijn den Reijer et al. showed that the larger angle of the jet flow in the BAV case from the normal TAV case can increase the aortic diameter and possibly cause a more severe dilatation [25]. According to a study by Della Corte et al. the site impacted by the BAV jet is found to have the highest probability of dilatation in the BAV cases [26]. Choudhury et al found that even though

TAV and BAV patients had the same maximum diameters of the ascending aorta, the BAV aortas were thinner than the TAV aortas. These findings may mean that BAV patients could have a higher risk of aortic dissection than TAV patients [27].

High dynamic pressure can cause complications to the aorta wall as well. Studies have been performed to find the differences in dynamic pressure between TAV and BAV leading to complications. One study by Santarpia et al. stated that there was higher dynamic pressure in the BAV than the normal TAV. This high dynamic pressure on an impact area can cause remodeling to the walls of the aorta [28].

As the mechanical stresses on the leaflets with BAV differ from the TAV it can be hypothesized that they could lead to diseases associated with BAV, such as calcification of the leaflets. According to Jermihov et al. the difference of maximum magnitudes of in-plane stresses between the BAV leaflets compared to the normal TAV leaflets could be as much as 161%. The stresses were highest at the attachments of the cusps in both the normal TAV and BAV cases, however, the magnitude of the stress was much higher for the BAV case. This higher stress may lead to calcification [8].

2.3 Computational Fluid Dynamic Studies

The results of the CFD aortic arch studies were similar to the results of the experimental curved arch studies. The velocity profile is shown to be skewed toward the inner wall during systole. Shahcheraghi states that this velocity profile is induced by the curved geometry itself and not by the flat inlet velocity condition [29]. Della Corte et al. studied CFD models and demonstrated that the BAV cusp restricted motion is enough to produce flow differentiation regardless of changing wall properties and increasing diameters [17]. CFD has been used to study WSS in the aortic arch. The results found

that the WSS is much higher in systole than during diastole [30]. Mori et al. found that the inner wall of the arch is more likely to experience high WSS [31]. Morris et al. also demonstrated that the WSS was highest along the inner wall as well and states that it is highest at the bend of the aortic arch [32].

CHAPTER THREE: METHODS

3.1 Geometry Development

Six idealized three dimensional geometries were developed in GAMBIT 2.4.6 (Fluent). The first geometry was an idealized aortic root with no valves. The second geometry was a normal TAV. Both of these cases were used as controls because it was not possible to tell whether the effect came from the arch geometry or the leaflets and because the TAV is the normal aortic valve geometry. Three types of idealized BAV geometries were created, Type I, Type II, and Type III. The final case of the six was the Type II geometry, the purely bicuspid valve, rotated ninety degrees.

The BAV geometries were constructed from a previously published model of a bioprosthetic heart valve as shown in Figure 3 [8]. The leaflets were created for an FE study by Jermihov et al. The dimensions of the TAV were similar to the physiological values of radius equal to 11.5 mm and height of 10.9 mm. The BAV geometries were created based on the normal TAV model but were modified to maintain dimensions similar to physiological values. Each type of BAV was modeled based qualitatively on surgical images and then idealized [8].
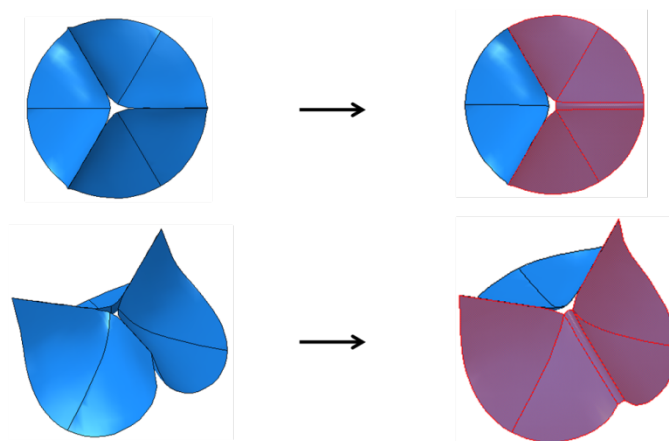

Figure 3. Left column represents the normal aortic valve geometry, and the right column highlights the altered geometry of BAV Type III [33]

Approximately 30 milliseconds into the cardiac cycle, the valve reaches its fully open configuration. This is referred to as peak systole. As we wanted to measure peak systolic flow in the aorta the coordinates from the previous models of the fully open geometry were exported and used to design the leaflets to be fixed in the fully open position. All six geometries had the same idealized ascending aortic root. This aortic root was designed by coordinates taken from Clark et al. [33].

The dimensions of the geometry are the following. The inlet diameter was .0229 meter. The outlet diameter was .0203 meter. The outlet was extended by .0254 meter to minimize reverse flow at the outlet

There were three Sinuses of Valsalva created for this simulation. These sinuses were constructed around idealized normal and pathological aortic valve geometries. The dimensions were comparable to the average dimensions of a normal human aorta [33]. The Sinuses of Valsalva varied slightly between the No Valve, TAV and BAV Type III cases and the BAV Types I and II cases. This was done to fit the sinuses to the specific leaflet geometry. Even with this change, variation was minimized to make sure the results were comparable. This difference also occurs in physiology as well. Figure 4a shows the idealized aortic root and ascending aortic geometries of the No valve and figure 4b shows the Type I BAV case.
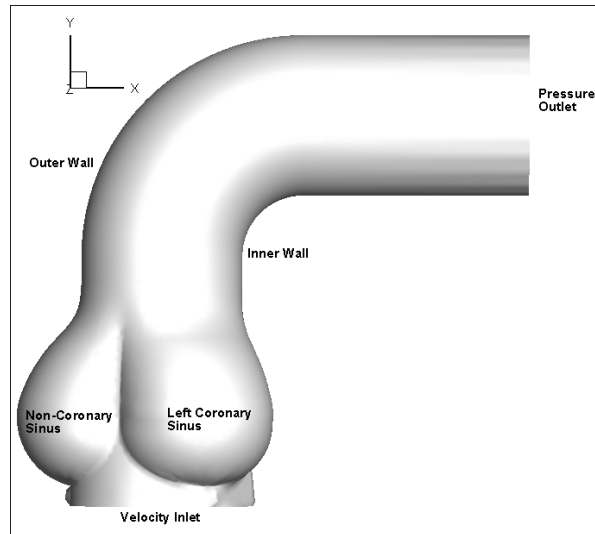
a)
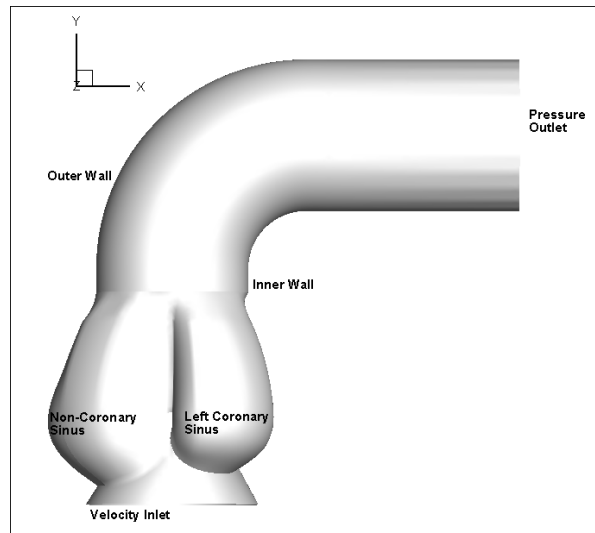
b)

Figure 4. The six idealized geometries a) No valve, TAV, BAV Type III root geometry b) BAV Types I and II root geometry

For this simulation the coronary arteries were not included since it was assumed that majority of the flow in the coronaries occur during diastole while this simulation is during systole [34]. The arterial bifurcations at the arch were also not included as our region of interest was confined to the ascending aortic segment.

The effective orifice areas (EOA) were calculated to make sure that the leaflet opening dimensions were correct for the TAV and BAV Types I, II, and III cases. Equation 1 by Gorlin was used to calculate the EOA [35]:

$$A = \frac{F}{44.5 \, C_d \sqrt{\Delta p}} \quad equation \; 1$$

where A is orifice area, F is the mean flow rate of blood in milliliters per second while the valve is open, Δp is the pressure gradient in millimeters of mercury and C_d is a discharge coefficient. For the aortic valve C_d is 1. The EOA for each case is listed in Table 1.

Table 1. The EOAs for all six cases in cm^2

	No Valve	TAV	BAVI	BAVII	BAVII-90	BAVIII
EOA (cm^2)	N/A	3.59	1.77	1.84	1.84	1.60

3.2 Mesh Generation

A three dimensional mesh was created in GAMBIT 2.4.6 (ANSYS INC). Volume elements must be present in a three dimensional mesh. Therefore, an unstructured tetrahedral mesh was generated inside the root geometry to ensure that volume elements were present. The interval size for the mesh on the edge was .032. GAMBIT defines the interval size between nodes by equation 2:

$$n = \frac{L}{d} \quad equation \; 2$$

where n is the number of nodes, L is the length of the edge, and d is the interval size [36]. Table 2 lists the number of nodes and tetrahedral cells that was generated by each mesh.

Table 2. The number of nodes and tetrahedral cells in each of the geometries

Types of Valves	Number of Nodes	Number of Tetrahedral Cells
No Valve	52667	273568
TAV	55384	289321
BAV Type I	63679	340493
BAV Type II	57533	306018
BAV Type II rotated 90 degrees	63495	341868
BAV Type III	63172	328871

3.3 Computational Fluid Dynamics

After meshing, the geometry was imported into Fluent 12.1.4 (ANSYS INC).

Fluent is governed by the continuity and Navier-Stokes equations. The continuity

equation for a three-dimensional analysis is given by equation 3 [37]:

$$\frac{\partial u}{\partial x} + \frac{\partial v}{\partial y} + \frac{\partial w}{\partial z} = 0 \quad equation\ 3$$

The Navier- Stokes equations for a three-dimensional analysis are given by

equations 4 through 6 [37]:

$$\rho\left[\frac{\partial u}{\partial t} + u\frac{\partial u}{\partial x} + v\frac{\partial u}{\partial y} + w\frac{\partial u}{\partial z}\right] = -\frac{\partial p}{\partial x} + \mu\left[\frac{\partial^2 u}{\partial x^2} + \frac{\partial^2 u}{\partial y^2} + \frac{\partial^2 u}{\partial z^2}\right] \quad equation\ 4$$

$$\rho\left[\frac{\partial v}{\partial t} + u\frac{\partial v}{\partial x} + v\frac{\partial v}{\partial y} + w\frac{\partial v}{\partial z}\right] = -\frac{\partial p}{\partial y} + \mu\left[\frac{\partial^2 v}{\partial x^2} + \frac{\partial^2 v}{\partial y^2} + \frac{\partial^2 v}{\partial z^2}\right] \quad equation\ 5$$

$$\rho\left[\frac{\partial w}{\partial t} + u\frac{\partial w}{\partial x} + v\frac{\partial w}{\partial y} + w\frac{\partial w}{\partial z}\right] = -\frac{\partial p}{\partial z} + \mu\left[\frac{\partial^2 w}{\partial x^2} + \frac{\partial^2 w}{\partial y^2} + \frac{\partial^2 w}{\partial z^2}\right] \quad equation\ 6$$

where ρ is density, μ is viscosity, and $\frac{\partial p}{\partial z}$ is change in pressure.

In using the Navier-Stokes equations to find an approximate solution in FLUENT

some assumptions must be followed. All geometries had the same assumptions,

parameters, and inputs. This ensured that the only variable in the experiment was the

change in leaflet geometry. The following assumptions were made: the fluid was incompressible, homogeneous and Newtonian; the walls and the leaflets were rigid. The no-slip condition was imposed at the fluid-solid interface. Since the fluid was assumed to be incompressible the density was kept constant [37]. Although blood is a non-Newtonian fluid, it can be assumed to be Newtonian during the forward flow phase with relatively large rates of shear in the CFD simulation [37]. The flow was also assumed to be a laminar unsteady flow. The laminar flow condition was verified by computing the Reynolds number and the critical Reynolds number. The Reynolds number is a dimensionless number that helps define if the flow is laminar or turbulent and is calculated by equation 7:

$$Re = \frac{\rho v d}{\mu} \quad equation\ 7$$

where ρ is the density of the fluid, v is the velocity of the fluid, d is the diameter, and μ is the viscosity of the fluid.

The Reynolds number for this simulation at the inlet was found to be 4868. Although any Reynolds number above 2100 can be turbulent in this case because it is below the critical Reynolds number of 5190, see equation 8, it is acceptable to use laminar flow condition [38]. The condition was shown by Nerem et al. that below the critical Reynolds number there are no flow disturbances and therefore the flow is laminar [38].

$$Re_c = constant * \alpha \quad equation\ 8$$

where constant is equal to 300, and α is the Womersley number defined in equation 9 [37].

$$\alpha = \frac{d}{2}\sqrt{\frac{\rho\omega}{\mu}} \quad equation\ 9$$

The Womersley number α computed from equation 9 is 17.3. The average

Womersley number in the ascending aorta is around 20 [37]. Since the numbers are close

the simulation can be assumed to correlate with realistic conditions.

The flow parameters were set for this simulation to act as realistically as possible.

The density of blood was a constant set to 1060 kg/m*s as the flow was assumed to be

incompressible as mentioned above. While viscosity isn't always constant for blood

when the shear rate is larger than 50-100 sec^{-1} the apparent viscosity becomes constant at

3.5 cP [37]. Therefore the viscosity in the aorta, which has a large shear rate, in this

simulation remained constant at 3.5 cP. The inlet was a uniform velocity inlet with the

velocity set at a constant .7 m/s. This inlet velocity allowed for a flow rate of 18 liters

per minute which has been found to be an average flow rate during peak systole [37].

The outlet was defined as a zero-pressure outlet. All other surfaces were set as walls.

The convergence level was set to 1 e -5. The scheme was set to SIMPLE and first-order

upwind. The time step size was .01 sec. This violates the Courant-Friedrichs-Lewy

(CFL) condition which is a dimensionless number that defines convergence through

keeping the time step small enough for information to move through the space. The CFL

number was found, by equation 10, to be .5 [39].

$$CFL = \frac{u * \partial t}{\partial x} \quad equation\ 10$$

where u is velocity, dt is the time step, and dx is the difference in length.

This violation is acceptable for this simulation in Fluent because of the implicit

scheme and the simulation being uncoupled. To make sure this was the case, three test

simulations were conducted with different time step sizes, one with a time step size of 2.64 e-6 that satisfies the CFL condition of .5, and two time step sizes of 5 and .01 that violate the CFL condition. These simulations showed minimal differences between the cases and therefore the time step size of .01 seconds was used as it would be sufficient to reach convergence in the shortest computational time. The simulation ran for 60 time steps which amounted to three passes through the geometry. After 60 time steps the results did not change this allowed us to believe that the solution had converged.

3.4 Post Processing

Post analysis was performed in Tecplot 360 (TECPLOT INC.). The axial velocity with units in meters/second was found at the STJ, streamlines were also found, as was the WSS contours with units in Pascal were found by equation 11, and dynamic pressure with units in Pascal was also found by equation 12:

$$\tau = \mu \frac{du}{dy} \quad equation\ 11$$

where τ is the wall shear stress, μ is viscosity and $\frac{du}{dy}$ is the change in velocity over the change in y [37].

$$q = \frac{1}{2}\rho v^2 \quad equation\ 12$$

where q is the dynamic pressure, ρ is the density and v is the velocity [40].

CHAPTER FOUR: RESULTS

4.1 Dynamic Pressure

The dynamic pressure, seen in Figures 5-10, found along the symmetrical z plane in all six cases. The plane was found by taking a slice through the z plane at the symmetrical axis. Two more slices were taken, one through the y plane at the STJ and a second slice through the arch. The legend is shown in the No Valve geometry, Figure 5. BAV Type I had the highest dynamic pressure along the inner wall while BAV Type III had the highest dynamic pressure along the outer wall. The BAV Type II cases show that dynamic pressure is also symmetrical about the center of the leaflet, as seen in figures 8 and 9.
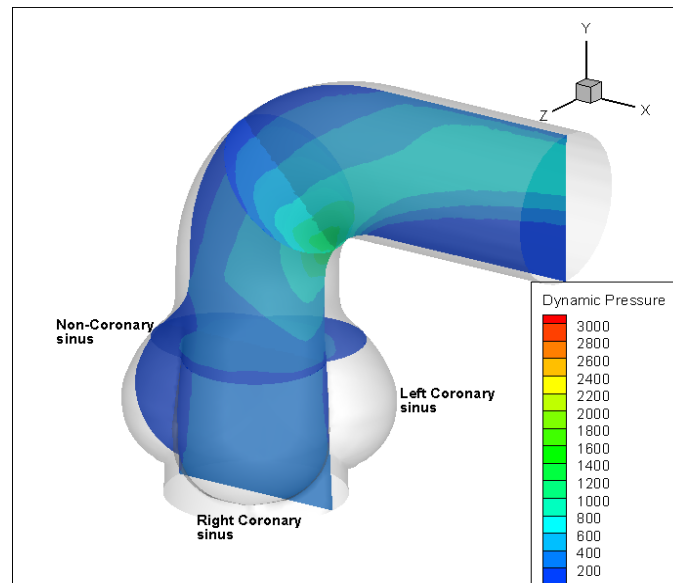

Figure 5. Dynamic Pressure in the symmetrical z plane with slices at the STJ and arch of the No valve geometry
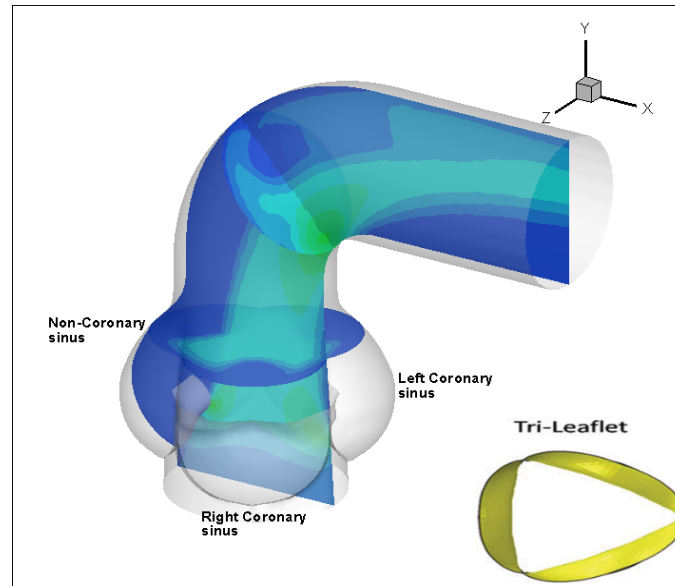
Figure 6. Dynamic Pressure in the symmetrical z plane with slices at the STJ and arch of the TAV geometry
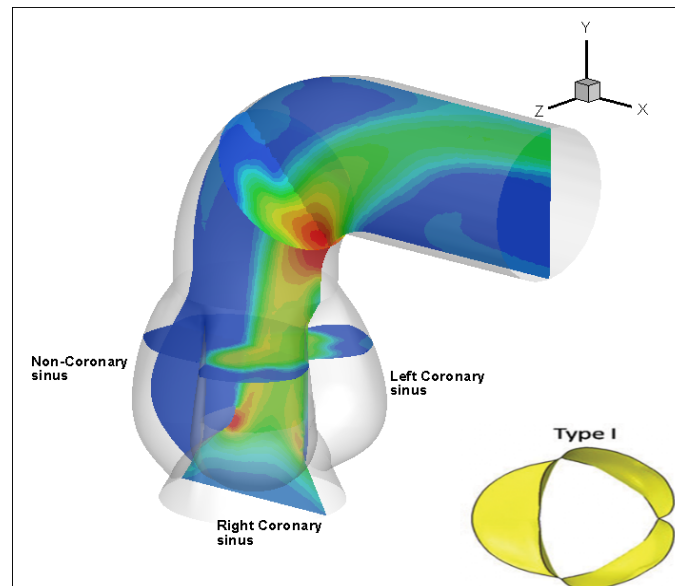

Figure 7. Dynamic Pressure in the symmetrical z plane with slices at the STJ and arch of the BAV Type I geometry
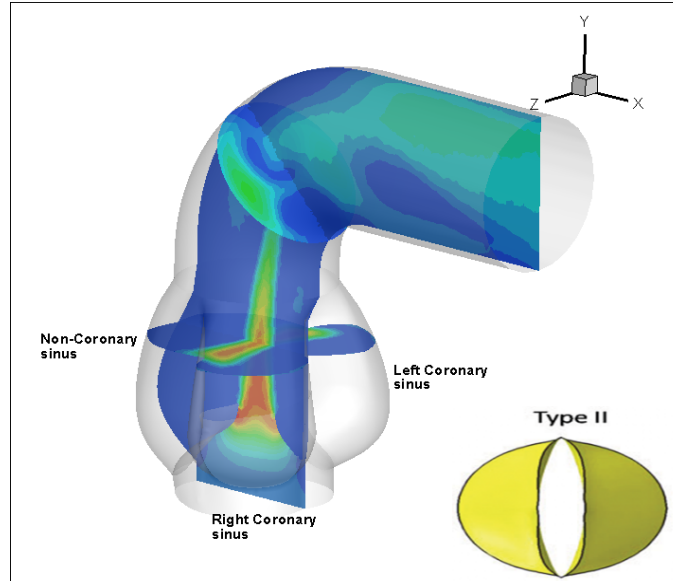
Figure 8. Dynamic Pressure in the symmetrical z plane with slices at the STJ and arch of the BAV Type II geometry
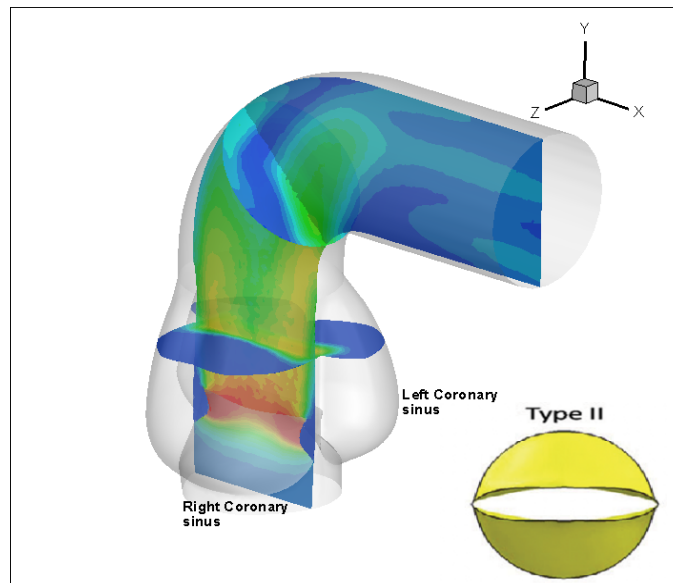

Figure 9. Dynamic Pressure in the symmetrical z plane with slices at the STJ and arch of the BAV Type II rotated 90 degrees geometry
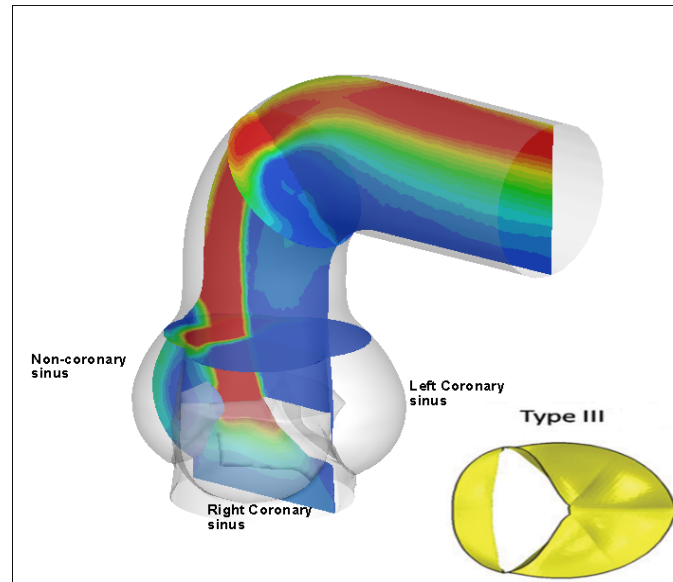
Figure 10. Dynamic Pressure in the symmetrical z plane with slices at the STJ and arch of the BAV Type III geometry

4.2 WSS Contours

Figures 11-16 show the WSS magnitude in contours. The WSS magnitude contours were taken in the axial direction for each of the six cases. The legend is shown in the No Valve geometry, figure 11. BAV Type I, seen in figure 13, had the highest magnitude of WSS along the inner wall. Figure 16 shows that BAV Type III had the lowest WSS magnitude along the inner wall and the highest magnitude of WSS along the outer wall. All BAV cases had lower WSS in the sinuses than the TAV case.
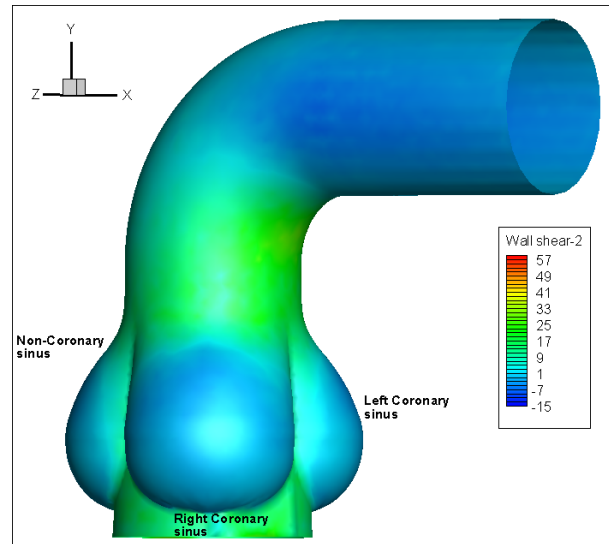
Figure 11. WSS Magnitude Contours for the No valve case
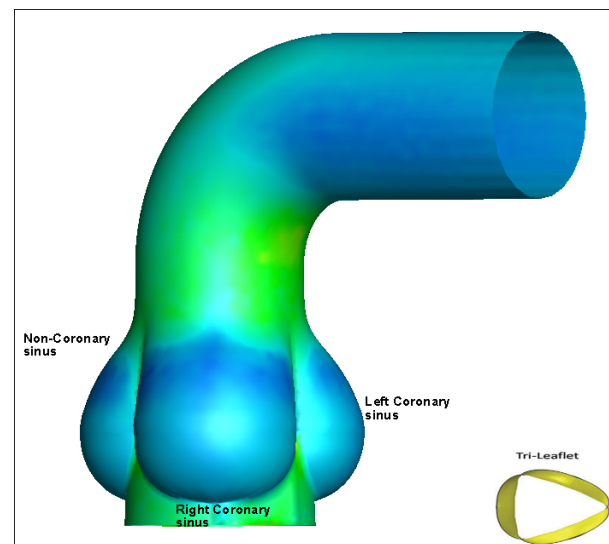
Figure 12. WSS Magnitude Contours of the TAV
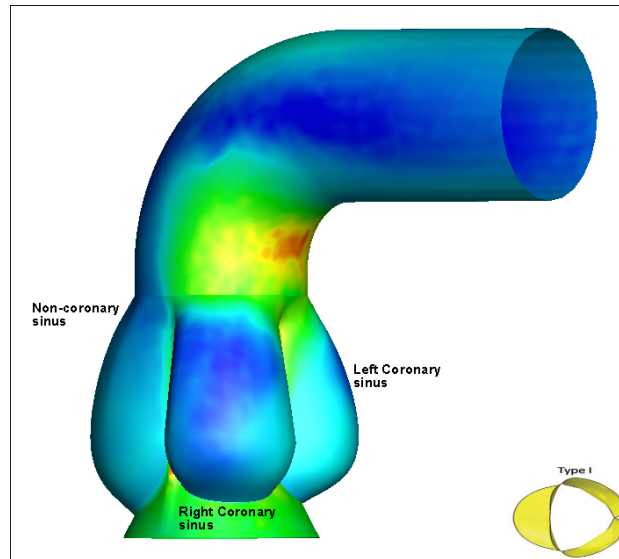
Figure 13. WSS Magnitude Contours for the BAV Type I case
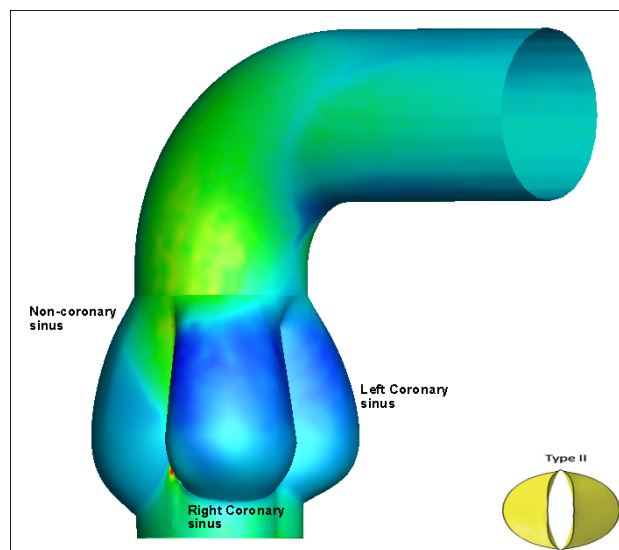
Figure 14. WSS Magnitude Contours for the BAV Type II case
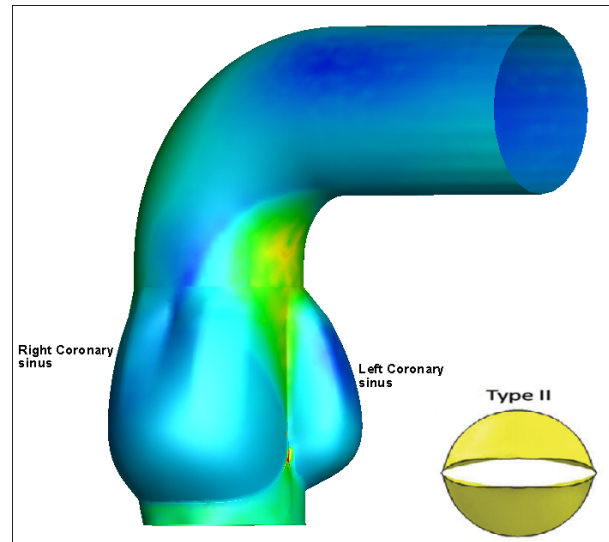
Figure 15. WSS Magnitude Contours of the BAV Type II rotated 90 degrees case
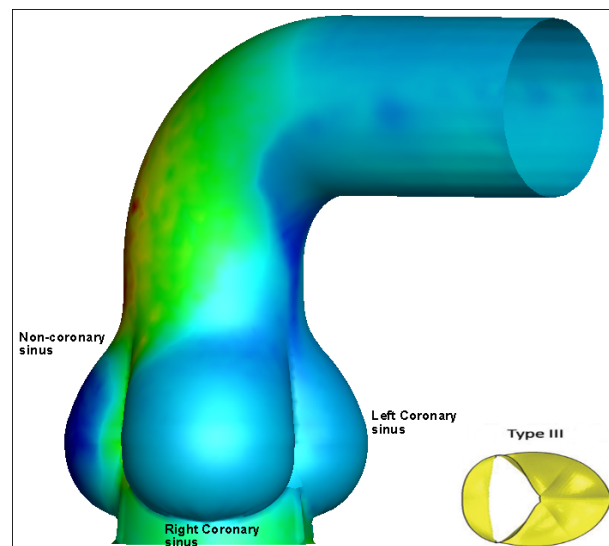
Figure 16. WSS Magnitude Contours for the BAV Type III case

4.3 WSS Graphs

Figures 17 and 18 show the inner and outer WSS in the axial direction. The first

point was taken at the STJ and the last point was after the arch. The points were

extracted from the center of the inner and outer walls. The position data was then

normalized.
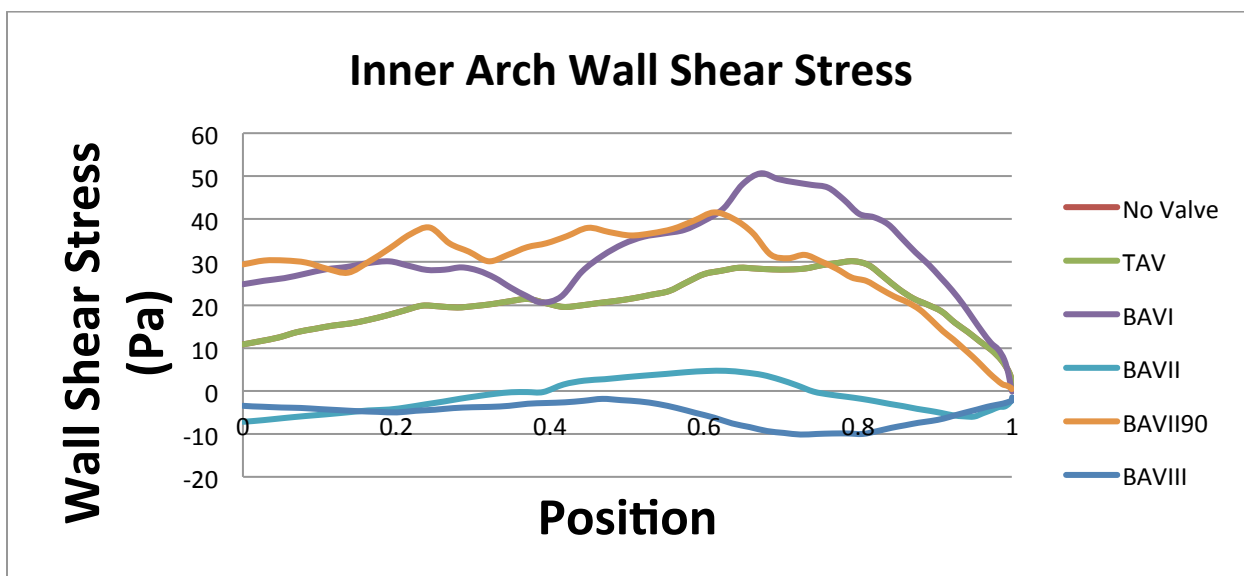
Figure 17. Position along inner arch in axial direction versus WSS magnitude
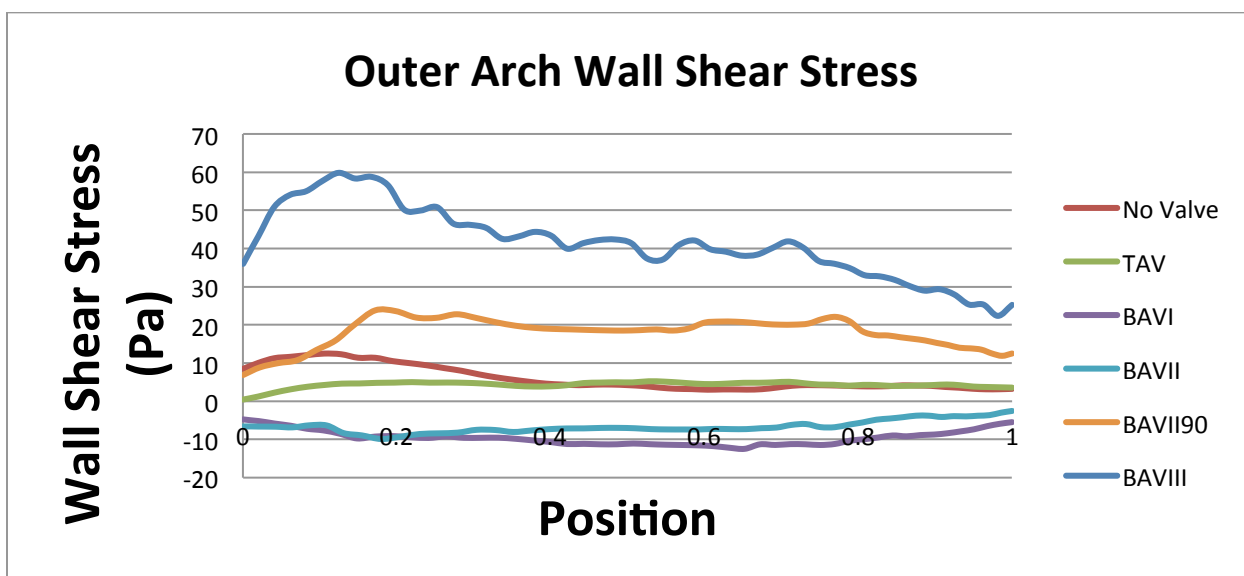
Figure 18. Position in axial direction versus outer arch WSS magnitude

<u>4.4 Velocity Profiles at STJ</u>

The Y Velocity was taken for each of the six cases. Figures 19-24 show this axial velocity from a slice in the y plane that was taken at the STJ. The figures also illustrate the velocity vectors in the y direction. The legend is shown in the No Valve case, figure 19. The axial velocity for the TAV case was fairly symmetrical about the leaflets. The BAV Type I was highly skewed toward the inner wall. The BAV Type III was highly skewed toward the outer wall. The BAV Type II cases were symmetrical and had the smallest jet with the greatest amount of circulation.
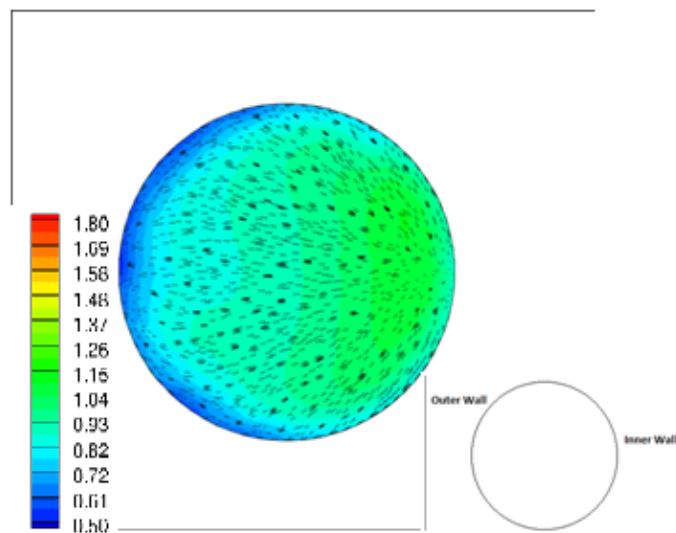
Figure 19. Velocity Profile at STJ for the No valve case
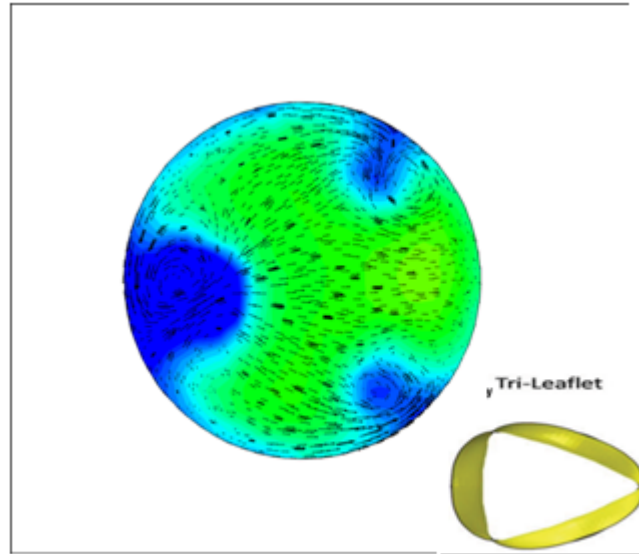
Figure 20. Velocity Profile at STJ of TAV
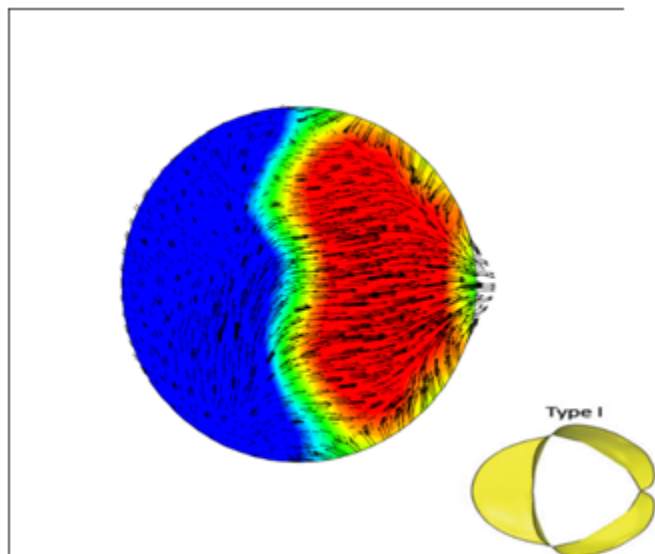
Figure 21. Velocity Profile at STJ for the BAV Type I case
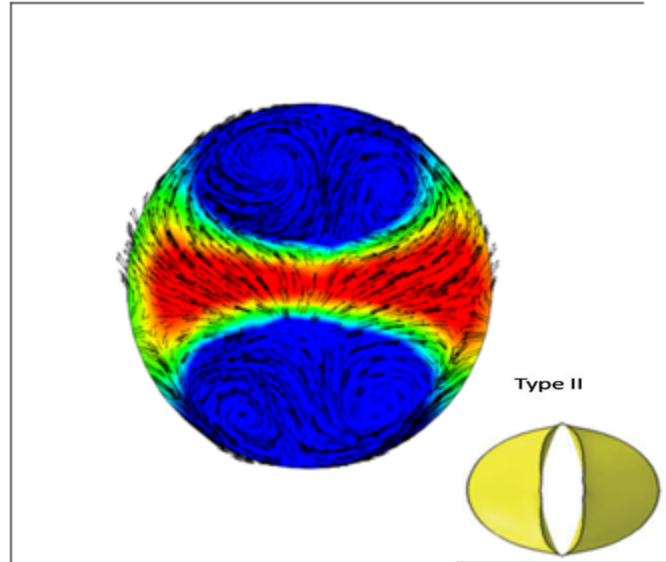
Figure 22. Velocity Profile at STJ for BAV Type II
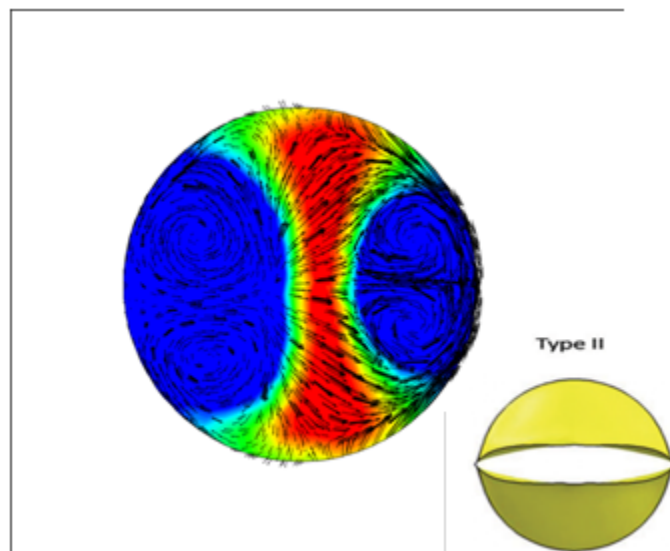
Figure 23. Velocity profile at STJ for BAV Type II rotated 90 degrees
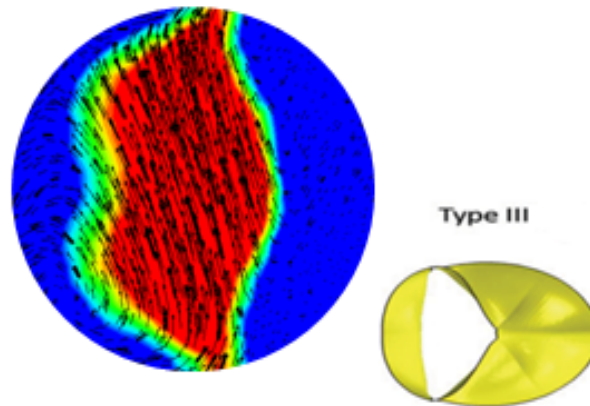
Figure 24. Velocity profile at STJ of Type III BAV

4.5 Streamlines

Figures 25-30 show the streamlines in the z plane. TAV, in figure 26, shows a slight skewing toward the inner wall. BAV Type I, in figure 27, shows the jet skewed, more than the TAV case, toward the inner wall of the arch. BAV Type II case, figures 28, shows a small jet in the center of the aorta. For figure 29, the BAV Type II streamlines are helical. In all cases the streamlines show recirculation in the sinuses. BAV Type III, shown in figure 30a, depicts the streamlines being skewed toward the outer wall and having a helical pattern along the inner wall. Figure 30b shows streamlines of a BAV from a study Della Corte et al. When comparing figures 30a and 30b it can be seen that there is a helical flow on the inner wall of the arch. There are also streamlines that are skewed toward the outer wall. Della Corte et al. hypothesized that this jet could lead to dilatation of the aortic wall at the impact site [17].
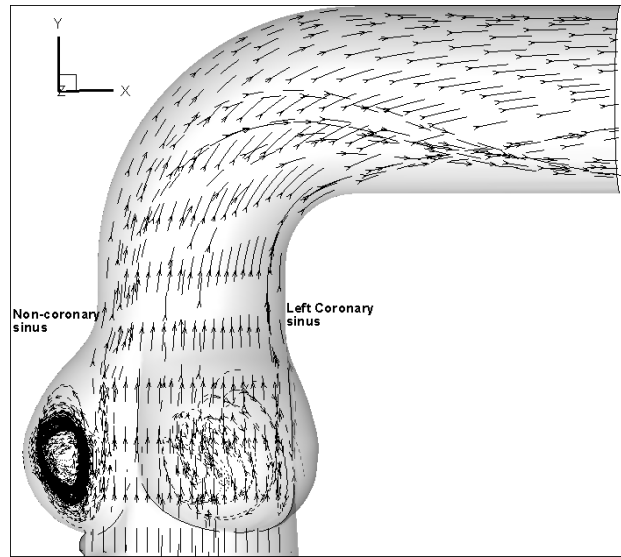
Figure 25. Streamlines in No valve case
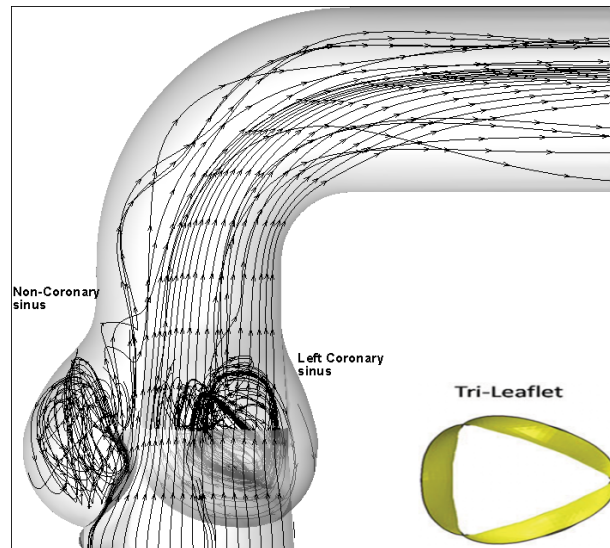
Figure 26. Streamlines for TAV
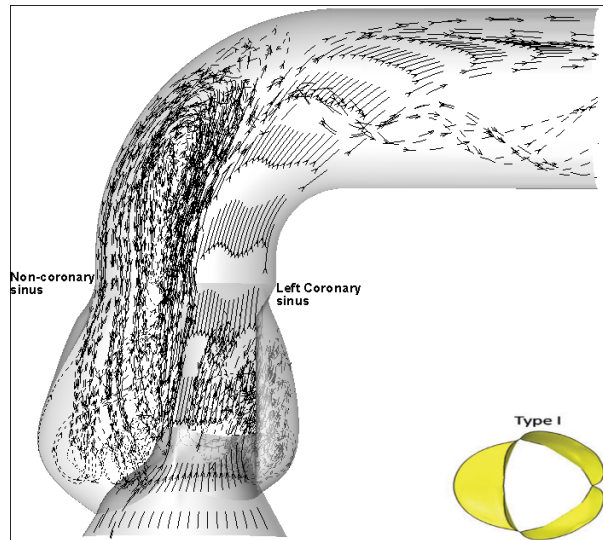
Figure 27. Streamlines of BAV Type I case
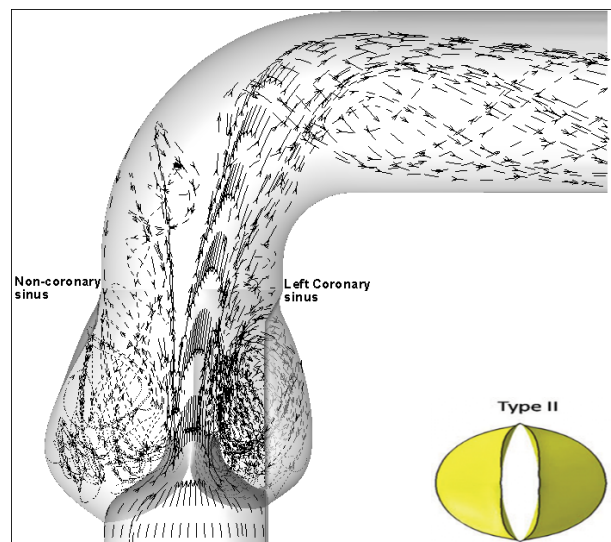
Figure 28. Streamlines of BAV Type II
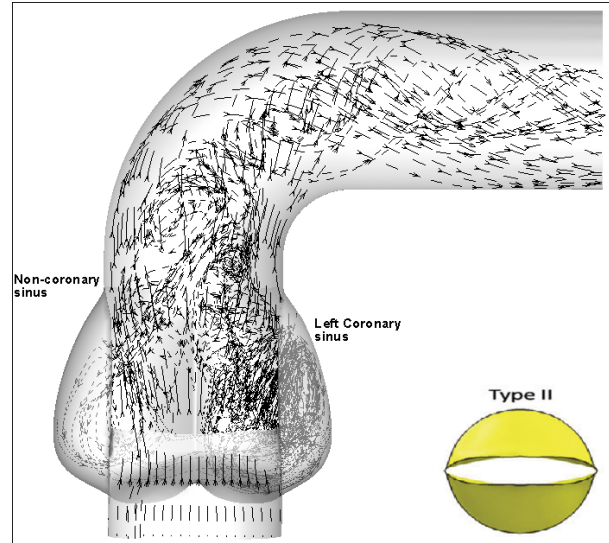
Figure 29. Streamlines of BAV Type II rotated 90 degrees
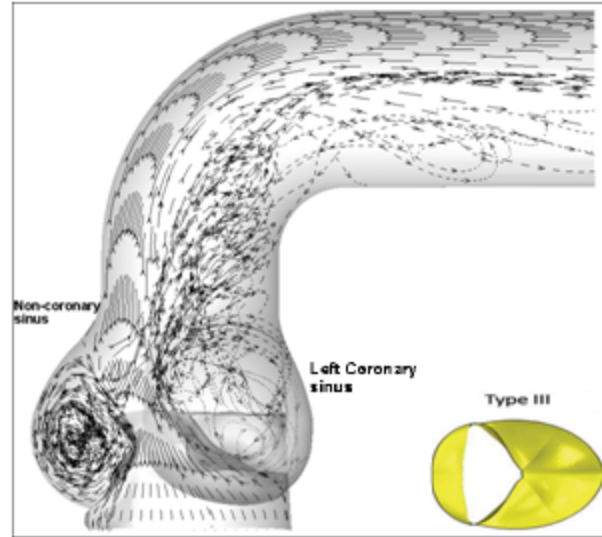
a)
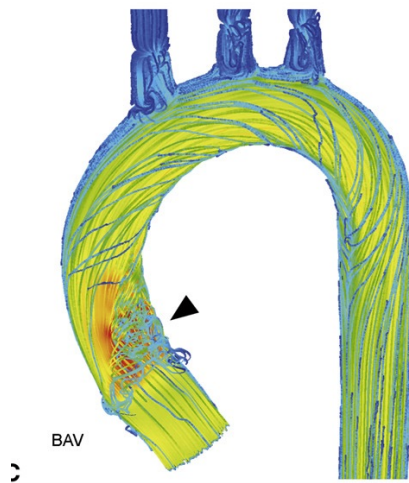
b)

Figure 30. Streamlines a) for our simulation for BAV Type III case b) from Della Corte et al. showing streamlines for BAV Type III [17]

CHAPTER FIVE: DISCUSSION AND LIMITATIONS

5.1 Discussion

Figures 5-10 show the dynamic pressure in all six cases. The dynamic pressure in the TAV control case, seen in figure 6, has its highest point at the inner wall near the bend of the arch; however, the magnitude of the pressure here is much less than for the BAV Type I.   Figure 7 shows BAV Type I has the highest dynamic pressure impacting on the inner wall at the bend of the arch.   As stated before high dynamic pressure can lead to remodeling of the aorta [28]. This remodeling may cause the wall to weaken and lead to an aortic dissection. Both BAV Type II geometries, in figures 8 and 9, can be seen to have a very pronounced jet BAV Type III, shown in figure 10, has the highest dynamic pressure against the outer wall of the arch and just after the non-coronary sinus. These results were similar to the study conducted by Della Corte et al. who found a jet that skewed toward just downstream of the non-coronary sinus. This jet was hypothesized to cause aortic dilatation [17]. This site is the most common site for dissection.   Contrufo et al. found wall changes at this same point *in-vivo* and hypothesized that this could be due to the eccentric asymmetric wall stress [41].

Another complication that results from BAV is the calcification of the leaflets [6]. BAV Type II cases (figures 8 and 9) have the highest dynamic pressure at the leaflets. Types I (figure 7) and III (figure 10) also show higher dynamic pressure at the leaflets compared to the TAV. Varying dynamic pressure has been shown to lead to stretch in the leaflets which could in turn lead to calcification of the leaflets [42]. The differences in dynamic pressure at the leaflets could lead to different calcification patterns between the TAV and BAV cases.

Figures 17 and 18 demonstrate the overall WSS magnitude trend for all geometries. This trend is that the inner WSS seems to be higher than the outer WSS except for the BAV Type III case. The contours in Figures 11-16 match the overall trend and show that the WSS for most geometries is highest along the inner wall. This is consistent with previous studies such as one by Leuprecht et al. [43].

BAV Type I has the highest magnitude of WSS along the inner wall which can be seen in figure 17 and can also be seen in the contour of WSS in figure 5. This is the same area where the dynamic pressure is the highest. The next highest average magnitude WSS for the inner wall as seen in figure 17 is the BAV Type II rotated 90 degrees. This makes sense as the jet is impacting the inner and outer walls directly. The TAV and No-leaflet cases were the next highest average WSS magnitude along the inner wall and did not differ in this region. This may mean that the geometry may have more of an effect on WSS then the leaflets themselves; however, the BAV Type I has a higher WSS therefore the bicuspid leaflets must play a role in this differentiation. The BAV Type II has a much lower average magnitude of WSS and in some places the WSS was negative. The final case BAV Type III has the lowest average WSS magnitude along the inner wall. This magnitude is negative along the whole inner wall. Many previous studies, such as Markl, were performed to show that low WSS has been linked to Arteriosclerosis [44]. Therefore BAV Types II and III have the highest risk of developing Arteriosclerosis along the inner wall of the aortic arch.

As can be seen by figure 18 the highest average WSS magnitude along the outer wall is the BAV Type III case. This WSS magnitude along the outer wall is significantly higher than all of the other cases. The high magnitude WSS could lead to aortic

dissection just after the non-coronary sinus as mentioned previously in a study by Della

Corte et al. [17]. The second highest is the BAV Type II rotated 90 degrees. Again the

jet and symmetry of the valve contributed to this WSS magnitude. The inner WSS in this

case was higher than the outer WSS which again leads to the idea that the geometry

contributes to a skew toward the inner wall   The No valve and TAV are very similar

although they do differ at the beginning region which is where the sinuses are located.

This region could be where the leaflets contribute more than the geometry. BAV Type I

and II both had negative WSS magnitudes with Type II having the lower average WSS

magnitude. As said before the low WSS in BAV Types I and II may lead to

Arteriosclerosis in these sites along the outer wall of the aortic arch [44].

The WSS is different in the sinuses as well, see figures 11-16. While the normal

TAV has some negative WSS values the BAV cases have lower negative WSS values in

the sinuses especially BAV Types I and III. BAV Types I and III vary in the location of

the negative values. BAV Type I has negative values in the Left and Right Coronary

Sinuses while BAV Type III has negative values in the Non-Coronary Sinus. This is

most likely due to recirculation in the sinuses.

The axial velocity profiles at the STJ show the differences in jet flow between the

six cases, see figures 19-24. As previous studies, including Schafer et at., have suggested

the jets may play a role in the differences in diseases [21]. Five of the six cases show the

velocity profiles skewing toward the inner wall. This has been seen in many studies

including a CFD study by Morris et al. also shows the skewing of the velocity toward the

inner wall [32]. The sixth case BAV Type III, see figure 22, does not skew toward the

inner wall but instead toward the outer wall. This is consistent with the previously reported data where the dynamic pressure and WSS are higher at the outer wall.

Although the velocity profile of the TAV, see figure 20, is skewing toward the inner wall it is still mostly symmetrical about the shape of the leaflets. In figure 21, BAV Type I has a high axial velocity that is skewed more than all other cases toward the inner wall of the aortic arch. The BAV Type II and BAV Type II rotated 90 degrees, see figures 22 and 23, are the same shape and magnitude as expected. They also have the smallest jet size of all cases which could lead to dissection along the wall where the jet hits.

Also seen in the velocity profiles, shown in figures 19-24 are the velocity vectors. These vectors show a minor circulation in the normal TAV; however, in the BAV cases there is much more circulation. BAV Type II has the highest amount of circulation with two vortices on each side of the jet. This circulation could cause the endothelial cells to be damaged from asymmetrical flow patterns which in could lead to dilatation [41].

The streamlines were also analyzed to visualize the direction of the flow as can be seen in figures 25-30. The only shortcoming of the streamlines is that the magnitude of velocity is not able to be visible. The streamline for the No valve case, figure 25, is relatively flat with minor recirculation in the sinuses. The TAV case, figure 26, showed a skewing toward the inner wall and recirculation in the sinuses as well. The BAV streamlines were much different than the control TAV and No valve cases.   BAV Type I, shown in figure 27, skews even more than the TAV toward the inner wall. Again this high impact along the inner wall could lead to dissection or dilatation. Along the outer wall of the BAV Type I is a major recirculation area that is much bigger than the TAV

and No valve recirculation, as these streamlines leave the sinus. The BAV Type II cases, figure 28 and 29, shows the streamlines through the leaflets as being very condensed in the middle of the geometry with a slight skew toward the inner wall. The sinuses have very high recirculation. BAV Type III, figure 30a, shows the streamlines being heavily skewed toward the outer wall. This skewing is also seen in figure 30b from Della Corte et al. who hypothesized that this jet could lead to aortic dilatation distal to the Non-Coronary Sinus [17]. This is the only case where the flow along the inner wall is helical. This helical streamline structure was similar to the previous study by Della Corte et al. whose results can be seen in figure 30b [17]. A helical streamline was also seen in a study by Hope et al. which hypothesized that exaggerated helical flow could lead to ascending aortic aneurysm [24].

5.2 Limitations

Due to time and computer constraints this study had many limitations. The geometries were idealized instead of patient specific as this was an initial simulation to assess the differences in the ascending aortic flow development with the commonly occurring BAV geometries. The use of patient specific data would make the simulation more realistic than using the idealized geometries. The mesh density was coarsened due to limitations in computational power and time taken to obtain a convergent solution employing a single workstation. In order to obtain highly resolved flow solutions, the mesh density must be significantly increased and will require parallelized CFD analysis involving multiple processor clusters. The Sinuses of Valsalva were changed for the BAV Type I and II cases to allow for correct geometry but may have led to more exaggerated results on the WSS within the sinuses. The leaflets were fixed at a fully

open geometry to simulate peak systolic flow. In order to observe the flow dynamics around moving leaflets fluid-structure interaction (FSI) technique would need to be utilized. In the body however the leaflets are moving which may cause additional complications.

CHAPTER SIX CONCLUSION

6.1 Conclusions

This study was able to evaluate the differences in flow development between the normal TAV and three types of BAVs using CFD. There were many differences in the dynamic pressure, WSS, velocity profiles and streamlines. This study was also able to compare these differences to the diseases that have been related through in-vivo studies to BAV. From these differences we can hypothesize that the BAV Type I would have the highest probability of disease, including dissection along the inner wall. The BAV Type III would have the highest probability aortic dissection and dilatation along the outer wall.

6.2 Clinical Impact

The results of this study will hopefully be useful in a clinical setting. A previous study by Fazel et al. stated that they found different categories for patterns of aortic dilatation that could lead to a custom approach to help BAV patients and physicians choose the correct course of treatment [45]. Similarly if the type of BAV can be identified the physician could use this current study to predict what disease may be most likely to occur and where it will occur for a specific type.

6.3 Future Work

The next step will be to correct for the limited time and computational space by refining the mesh density. This finer mesh will allow for the correction of results that may have occurred due to the coarse mesh density. Looking at the different times in the cardiac cycle, besides only the peak systolic, may help to see the variation in wall

disturbance. FSI will be utilized to look at the flow field around moving leaflets. The

final step will then be to use patient specific data to allow for more realistic conditions.

REFERENCES

[1] K. Chandran, "Flow Dynamics in the Human Aorta," *Journal of Biomedical Engineering,* vol. 115, pp. 611-16, 1993.

[2] "Healthy Living," 2012. [Online]. Available: http://healthy-lifestyle.most-effective-solution.com/2010/08/27/human-anatomy-aorta/. [Accessed 01 06 2012].

[3] J. M. Karamichalis, L. A. Vricella, D. J. Murphy and B. A. Reitz, "Simplified Technique for Correction of Anomalous Origin of Left Coronary Artery From the Anterior Aortic Sinus," *Ann Thorac Surg,* vol. 76, pp. 266-67, 2003.

[4] A. Vegas, Perioperative Two-Dimensional Transeophageal Echocardiography, New York: Springer, 2012.

[5] J. EDWARDS, "Editorial: The Congenital Bicuspid Aortic Valve," *Circulation,* vol. 23, pp. 485-88, 1961.

[6] N. Yener, L. Oktar, D. Erer, M. Yardimci and A. Yardimci, "Bicuspid Aortic Valve," *Ann Thorac Cardiovasc Surg,* vol. 8, pp. 264-67, 2002.

[7] P. Fedak, S. Verma, T. David, R. Leask, R. Weisel and J. Butany, "Clinical and Pathophysiological Implications of a Bicuspid Aortic Valve," *Circulation,* vol. 106, pp. 900-04, 2002.

[8] P. N. Jermihov, L. Jia, M. S. Sacks, R. C. Gorman, J. H. I. Gorman and K. B. Chandran, "Effect of Geometry on the Leaflet Stresses in Simulated Models of Congenital Bicuspid Aortic Valves," *Cardiovascular Engineering and Technology,* vol. 2, pp. 48-56, 2011.

[9] H.-H. Sievers and C. Schmidtke, "A classification system for the bicuspid aortic valve from 304 surgical specimens," *J Thorac Cardiovasc Surg,* vol. 133, pp. 1226-33, 2007.

[10] F. Robicsek, M. J. Thubrikar, J. W. Cook and B. Fowler, "The Congenitally Bicuspid Aortic Valve: How Does It Function? Why Does It Fail?," *Ann Thorac Surg,* vol. 77, pp. 177-85, 2004.

[11] W. Edwards, D. Leaf and J. Edwards, "Dissecting Aortic Aneurysm Associated with Congenital Bicuspid Aortic Valve," *Circulation,* vol. 57, pp. 1022-1025, 1978.

[12] S. Nistri, M. Sorbo, M. Marin, M. Palisi, R. Scognamiglio and G. Thiene, "Aortic root dilatation in young men with normally functioning bicuspid aortic valves," *Heart,* vol. 82, pp. 19-22, 1999.

[13] F. Gao and T. Matsuzawa, "FSI within Aortic Arch Model over Cardiac Cycle and Influence of Wall Stiffness on Wall Stress in Layered Wall," *Engineering Letters,* vol. 13, pp. 167-172, 2006.

[14] D. Nathan, C. Xu, J. Gorman, R. Fairman, J. Bavaria, R. Gorman, K. Chandran and B. Jackson, "Pathogenesis of Acute Aortic Dissection: A Finite Element Stress Analysis," *Ann Thorac Surg,* vol. 91, pp. 458-63, 2011.

[15] M. Cecconi, M. Marnfrin, A. Moraca, R. Zanoli, P. L. Colonna, M. G. Bettuzzi, S. Moretti, D. Gabrielli and G. P. Perna, "Aortic Dimensions in Patients With Bicuspid Aortic Valve Without Significant Valve Dysfunction," *The American Journal of Cardiology,* vol. 95, pp. 292-94, 2005.

[16] C. Ward, "Clinical significance of the bicuspid aortic valve," *Heart,* vol. 83, pp. 81-85, 2000.

[17] A. Della Corte, C. Bancone, C. Conti, E. Votta, A. Radaelli, L. Del Viscovo and M. Cotrufo, "Restricted cusp motion in right-left type of bicuspid aortic valves: A new risk marker for aortopathy," *J Thorac Cardiovasc Surg,* vol. 142, pp. 1-10, 2011.

[18] K. Chandran, "Role of Computational Simulations in Heart Valve Dynamics and Design of Valvular Prostheses," *Cardiovascular Engineering and Technology,* vol. 1, pp. 18-38, 2010.

[19] A. Harloff, A. NuBbaumer, S. Bauer, A. F. Stalder, A. Frydrychowicz, C. Weiller, J. Hennig and M. Markl, "In Vivo Assessment of Wall Shear Stress in the Atherosclerotic Aorta Using Flow-Sensitive 4D MRI," *Magnetic Resonance in Medicine,* vol. 63, pp. 1529-36, 2010.

[20] A. Barker, C. Lanning and R. Shandas, "Quantification of Hemodynamic Wall Shear Stress in Patients with Bicuspid Aortic Valve Using Phase-Contrast MRI," *Ann Biomed Eng.,* vol. 38, pp. 788-800, 2010.

[21] B. Schaefer, M. Lewin, K. Stout, E. Gill, A. Prueitt, P. Byers and C. Otto, "The bicuspid aortic valve: an integrated phenotypic classification of leaflet morphology and aortic root shape," *Heart,* vol. 94, pp. 1634-38, 2008.

[22] E. J. Weinberg and M. R. Kaazempur Mofrad, "A multiscale computational comparison of the bicuspid and tricuspid aortic valves in relation to calcific aortic stenosis," *Journal of Biomechanics,* vol. 41, pp. 3482-87, 2008.

[23] J. F. J. LaDisa, C. A. Taylor and J. A. Feinstein, "Aortic coarctation: Recent developments in experimental and computational methods to assess treatments for this simple condition," *Progress in Pediatric Cardiology,* vol. 30, pp. 45-9, 2010.

[24] M. D. Hope, T. A. Hope, A. K. Meadows, K. G. Ordovas, T. H. Urbania, M. T. Alley and C. B. Higgins, "Bicuspid Aortic Valve: Four-dimensional MR Evaluation of Ascending Aortic Systolic Flow Patterns," *Radiology,* vol. 255, pp. 53-61, 2010.

[25] P. Martijn den Reijer, D. I. Sallee, P. van der Velden, E. Zaaijer, W. J. Parks, S. Ramamurthy, T. Q. Robbie, G. Donati, C. Lamphier, R. P. Beekman and M. E. Brummer, "Hemodynamic predictors of aortic dilatation in bicuspid aortic valve by velocity-encoded cardiovascular magnetic resonance," *Journal of Cardiovascular Magnetic Resonance,* vol. 12, pp. 2-13, 2010.

[26] A. Della Corte, C. Quarto, C. Bancone, C. Castaldo, F. Di Meglio, D. Nurzynska, L. S. De Santo, M. De Feo, M. Scardone, S. Montagnani and M. Contrufo, "Spatiotemporal patterns of smooth muscle cell changes in ascending aortic dilatation with bicuspid and tricuspid aortic valve stenosis: Focus on cell–matrix signaling," *J Thorac Cardiovasc Surg,* vol. 135, pp. 8-18, 2008.

[27] N. Choudhury, O. Bouchot, L. Rouleau, D. Tremblay, R. Cartier, J. Butany, R. Mongrain and R. L. Leask, "Local mechanical and structural properties of healthy and diseased human ascending aorta tissue," *Cardiovascular Pathology,* vol. 18, pp. 83-91, 2009.

[28] G. Santarpia, G. Scognamiglio, G. Di Salvo, M. D'Alto, B. Sarubbi, E. Romeo, C. Indolfi, M. Cotrufo and R. Calacro, "Aortic and left ventricular remodeling in patients with bicuspid aortic valve without significant valvular dysfunction: A prospective study," *Int J Cardiol,* vol. 146, pp. 1-6, 2011.

[29] N. Shahcheraghi, H. Dwyer, A. Cheer, A. Barakat and T. Rutaganira, "Unsteady and Three-Dimensional Simulation of Blood Flow in the Human Aortic Arch," *Journal of Biomechanical Engineering,* vol. 124, pp. 378-87, 2002.

[30] S. Jin, J. Oshinski and D. P. Giddens, "Effects of Wall Motion and Compliance on Flow Patterns in the Ascending Aorta," *Journal of Biomechanical Engineering,* vol. 125, pp. 347-54, 2003.

[31] D. Mori and T. Yamaguchi, "Computational Fluid Dynamics Modeling and Analysis of the Effect of 3-D Distortion of the Human Aortic Arch," *Computer Methods in Biomechanics and Biomedical Engineering,* vol. 5, pp. 249-60, 2002.

[32] L. Morris, P. Delassus, A. Callanan, M. Walsh, F. Wallis, P. Grace and T. McGloughlin, "3-D Numerical Simulation of Blood Flow Through Models of the Human Aorta," *Journal of Biomechanical Engineering,* vol. 127, pp. 767-75, 2005.

[33] R. Clark and W. Swanson, "Dimensions and geometric relationships of the human aortic valve as a function of pressure," *Circ Res,* vol. 35, pp. 871-82, 1974.

[34] A. Y. K. Wong, J. Armour and K. B. Lee, "The dynamics of the coronary venous system in the dog," *Journal of Biomechanics,* vol. 17, pp. 173-183, 1984.

[35] R. Gorlin and S. Gorlin, "Hydraulic formula for calculation of the area of the stenotic mitral valve, other cardiac valves, and central occluding shunts," *Am Heart J,* vol. 41, pp. 1-29, 1951.

[36] "Fluent Incorportated," Fluent, Inc., 03 05 2000. [Online]. Available: http://202.118.250.111:8080/fluent/Gambit13_help/modeling_guide/mg0302.htm. [Accessed 13 05 2012].

[37] K. B. Chandran, A. P. Yoganathan and S. E. Rittgers, Biofluid Mechanics: The Human Circulation, Boca Raton: CRC Press, 2007.

[38] R. M. Nerem, W. A. Seed and N. B. Wood, "An experimental study of the velocity distribution and transition to turbulence in the aorta," *J. Fluid Mech.,* vol. 52, pp. 137-60, 1972.

[39] R. Courant, K. O. Friedrichs and H. Lewy, "Uber die Partiellen Differenzengleichuizgen der Mafhematischen Physik," *Math. Ann.,* vol. 100, pp. 32-74, 1928.

[40] T. Benson, "Dynamic Pressure," 18 June 2009. [Online]. Available: http://www.grc.nasa.gov/WWW/k-12/airplane/dynpress.html. [Accessed 13 May 2012].

[41] M. Contrufo, et al. "Different patterns of extracellular matrix protein expression in the convexity and the concavity of the dilated aorta with bicuspid aortic valve: Preliminary results," *J Thorac Cardiovasc Surg,* vol. 130, pp. 504-11, 2005.

[42] M. Weiler, C. Hwai Yap, K. Balachandran, M. Padala and A. P. Yoganathan, "Regional analysis of dynamic deformation characteristics of native aortic valve leaflets," *Journal of Biomechanics,* vol. 44, pp. 1459-65, 2011.

[43] A. Leuprecht, S. Kozerke, P. Boesiger and K. Perktold, "Blood flow in the human ascending aorta: a combined MRI and CFD study," *Journal of Engineering Mathematics,* vol. 47, pp. 387-404, 2003.

[44] M. Markl, F. Wegent, T. Zech, S. Bauer, C. Strecker, M. Schumacher, C. Weiller, J. Hennig and A. Harkiif, "In-vivo Wall Shear Stress Distribution in the Carotid Artery: Effect of Bifurcation Geometry, Internal Carotid Artery Stenosis and Recanalization Therapy," *Circ Cardiovasc Imaging,* vol. 3, pp. 647-55, 2010.

[45] S. S. Fazel, H. R. Mallidi, R. S. Lee, M. P. Sheehan, D. Liang, D. Fleischman, R. Herfkens, R. S. Mitchell and D. C. Miller, "The aortopathy of bicuspid aortic valve disease has distinctive patterns and usually involves the transverse aortic arch," *J Thorac Cardiovasc Surg,* vol. 135, pp. 901-7, 2008.